Mid-infrared all solid state DIAL for remote sensing of hazardous chemical agents

V. Vaicikauskas[a], Z. Kuprionis[b], M. Kaucikas[a,b], V.Svedas[a], V. Kabelka[a]
[a] Institute of Physics, Savanoriu 231, LT-02300 Vilnius, Lithuania, E-mail: vikvai@ktl.mii.lt
[b] EKSPLA, Ltd, Savanoriu 231, LT-02300 Vilnius, Lithuania

ABSTRACT

We describe all solid state differential absorption lidar (DIAL) based on the mid-infrared (IR) tunable Optical Parametric Oscillator (OPO). Generation of tunable mid-infrared laser radiation using a two stage tandem OPO was demonstrated. The first stage was based on the nonlinear KTP crystal and produced up to 45 mJ of 1.57 μm radiation, while pumped by a commercial Q-switched Nd:YAG laser. The quality of signal beam was improved by the use of unstable resonator. The $AgGaSe_2$ crystal was used in the second stage OPO. Idler energies up to 1 mJ were generated at this stage within tuning range from 6 to 12 μm. The receiver consisted of a 250 mm gold mirror telescope, two channel detection system and control electronics. We have designed a photoacoustic cell for wavelength calibration of lidar. Preliminary lidar field test results are presented.

Keywords: Remote sensing; hazardous gases; OPO; all solid state laser; mid-infrared DIAL

1. INTRODUCTION

Public awareness of atmospheric pollution by hazardous and greenhouse gases is increasing on a global scale. As a result demand for trace gas detection devices and systems is also increasing. The range of devices under demand is very large: from light portable devices to large stationary systems, from one point monitoring to stand-off detection, from highly sensitive and calibrated systems to simple "Go/Don't Go" detectors. Nowadays, current technologies do not provide cost-effective solutions for such broad spectrum applications. Infrared (IR) molecular spectroscopy is a selective and sensitive tool for analysis of various gases and vapors. However, due to strong absorbency of atmospheric water and other gases large distance analysis could be performed only in the atmospheric transparency windows.
Various lidar systems are applied for remote sensing of different parameters of the atmosphere over recent 30 years [1, 2]. A differential absorption lidar is a powerful technique for remote detection of chemical gases in the atmosphere [3]. Lidars based on the CO_2 laser were used as "workhorses" for operating in the mid-infrared spectral region (near 10 μm) till now [4-6]. A mid-infrared spectral region is very attractive because characteristic molecular vibrations of all atmospheric pollutants are in this "molecular finger-print" region.
The laser source suitable for DIAL applications in the atmosphere should meet several requirements, most important ones being sufficient energy, good beam quality, and continuous wavelength tuning in IR (6 – 12 μm) range as well as reliability and stability. Traditional mid-IR sources for "fingerprint" spectral region were CO and CO_2 gas lasers. Using the CO_2 laser in lidars involves advantages as well as disadvantages. The main advantage of using CO_2 laser in lidars is possibility to get extremely large laser radiation energy (up to several joules). This is an important parameter for mid-infrared lidar systems, and allow geting sufficient signals regardless of smaller scattering cross-section of molecules in this spectral region. The disadvantages are narrow tuning spectral range (9-11μm) and discrete wavelength tuning of laser radiation (about 100 selective spectral lines) and they are large and heavy.
The present state of the art in the continuously tunable lasers suitable for chemical sensing in the mid infrared includes diode lead salt or quantum cascade lasers and sources based on nonlinear conversion. Lead salt lasers exibit shortcomings in power, beam quality, a very limited range of wavelength tuning and spectral reproducibility that can affect performance. They are more often used in indoor measurement systems such as multipass or photoacoustic cells. Quantum cascade lasers [7] is promising as an alternative that is free from some of these problems. QCLs have been shown to produce significant output power while maintaining single-longitudinal-mode operation. To date, however, QCLs exibit tuning over only a spectral width of about $10cm^{-1}$ and generally require cryogenic cooling. A room

Laser Radar Technology and Applications XI, edited by Gary W. Kamerman, Monte D. Turner,
Proc. of SPIE Vol. 6214, 62140E, (2006) · 0277-786X/06/$15 · doi: 10.1117/12.665638

temperature operation has been demonstrated in a buried heterostructure laser [8]. Moreover, diode lasers are limited in the choise of output that they provide – for example IR diode lasers cannot produce high-energy pulses that are required for use in a lidar.

Optical parametric oscillator (OPO) laser sources overcome drawbacks of CO_2 lasers. They offer wide mid-infrared wavelength tuning, while their size, beam quality and energy are still acceptable. Recently, very attractive all solid state DIAL system based on continuous wavelength tuning OPO in the spectral region up to 4.5 μm has been designed and demonstrated in field experiments [9].

In this paper, we present a spectroscopic trace gas detection system based on the mid-IR tandem OPO source. This system consists of the photoacoustic spectrometer and lidar. The photoacoustic spectrometer is built to detect low concentrations of trace gases and its main aim is high sensitivity point monitoring or unknown gas identification and calibration. The main objective of the lidar based open path system is remote sensing of trace gases and area monitoring. Combined these two devices form a powerful tool for atmospheric monitoring. In our opinion, this system is the first mid-IR tandem OPO source based system, which successfully combines sensitive point monitoring and stand-off detection while being compact, simple and cost-effective. Now the lidar system is under construction and should be finished in 2006.

2. EXPERIMENTAL IMPLEMENTATION

2.1. Development of tandem mid-IR OPO.

The mid-IR laser source is based on the tandem OPO scheme (Fig. 1). The pump source was a commercial Nd:YAG actively Q-switched nanosecond laser (NL303G, Ekspla Ltd). This pump laser produced up to 500 mJ of 1.064 μm pulsed (duration 3-6 ns) radiation and the profile of the beam was hat-top. The half-wave plates λ/2, polarizers P1, P2, Faraday rotator FR were applied to avoid back reflections from OPO to the pump laser. Then the radiation was directed to the first OPO cavity by two steering mirrors M1 and M2. The beam diameter was compressed by the telescope consisting of lenses L1 and L2.

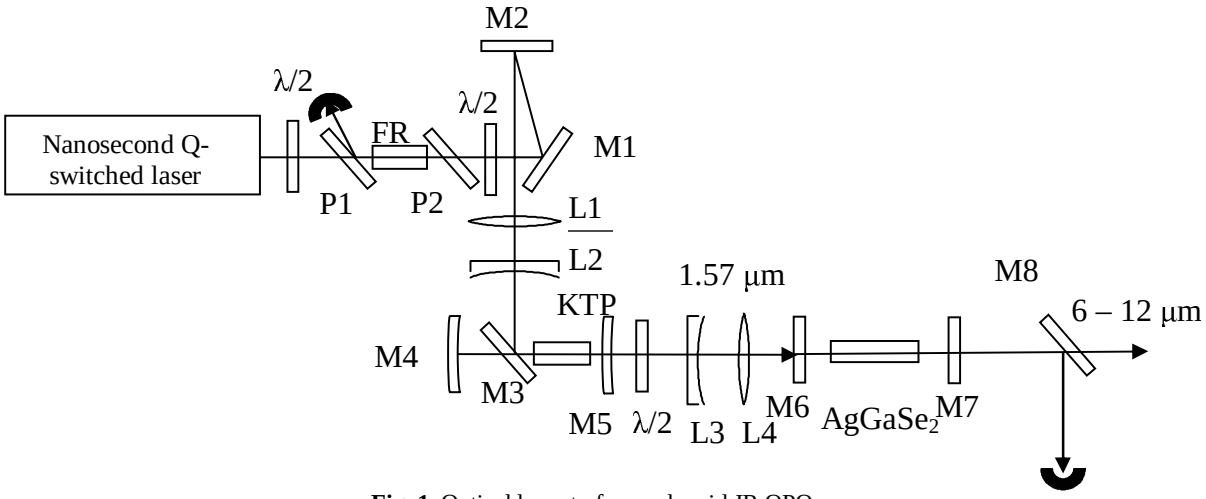

Fig. 1. Optical layout of cascade mid-IR OPO.

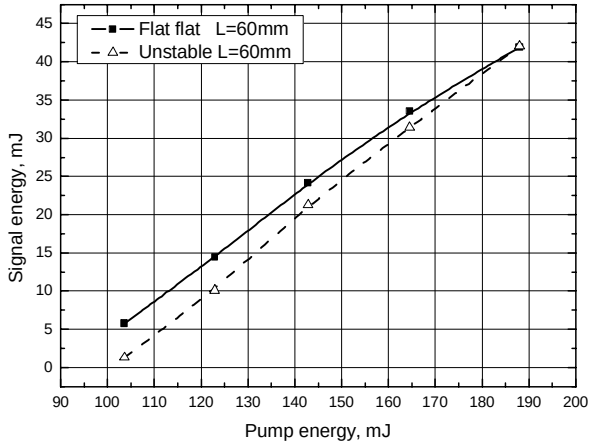

Fig.2. Signal energy dependence on pump energy at the first stage of OPO

The first stage of OPO was based on the KTP (5x5x25 mm^3) nonlinear crystal (EKSMA, Ltd). The crystal was anti-reflection coated for 1.064 and 1.57 μm wavelengths and was cut at $\theta = 90^o$, $\varphi = 0^o$ (x-cut). This allowed noncritical phase-matching (II type) at 1.57 μm when pumped by 1.064 μm radiation. The first stage OPO cavity was singly-resonant for signal wave. Two sets of mirrors M4 and M5 were used for the first stage OPO. The first set consisted of two flat mirrors. The rear mirror was highly reflective at 1.57 μm and no special coatings for other wavelengths were used. The output coupler was highly reflective at pump wavelength and 50% reflective at signal radiation. The second set of mirrors consisted of two spherical mirrors. The radius of the curvature of the concave rear mirror was 40 cm and that of the convex output coupler was -30 cm. The latter was made as a zero meniscus lens. This choice of mirrors resulted in unstable positive-branch cavity with magnification factor M = 1.33.

The output energy dependence on pump energy of the first stage OPO is presented in Fig. 2. Threshold intensity was about 100÷130 MW/cm^2 for both flat-flat and unstable resonators. As it can be seen in Fig. 2, signal energies are higher in flat-flat case than in the unstable one when pump energy is about 110 mJ. As pump energy increases, the difference becomes smaller and it vanishes at 190 mJ pump energies. So at high pump energies, there is very little difference between the cavities as far as generated energy is concerned.

The divergence of generated radiation was 4.5 mrad and 3.2 mrad in a flat-flat and unstable cavity, respectively. The improvement in the divergence for an unstable cavity was enough to pump the second stage of tandem OPO system, as it is shown below.

The second stage of the tandem OPO system was based on the $AgGaSe_2$ nonlinear crystal (8x10x20 mm^3). This crystal was cut for I type critical phase-matching in 6÷12 μm range, when pumped at 1.57 μm. The second stage OPO cavity was also singly resonant for signal wave (1.8÷2.2 μm). The cavity consisted of two flat mirrors: the rear mirror was highly transmitting at 1.57 μm and highly reflective in 1.8÷2.2 μm range, whereas the output coupler reflected 50% of 1.8÷2.2 μm radiation and was highly transmitting in the 6÷12 μm range. A separator was placed outside the OPO cavity to separate pump and signal waves from an idler wave.

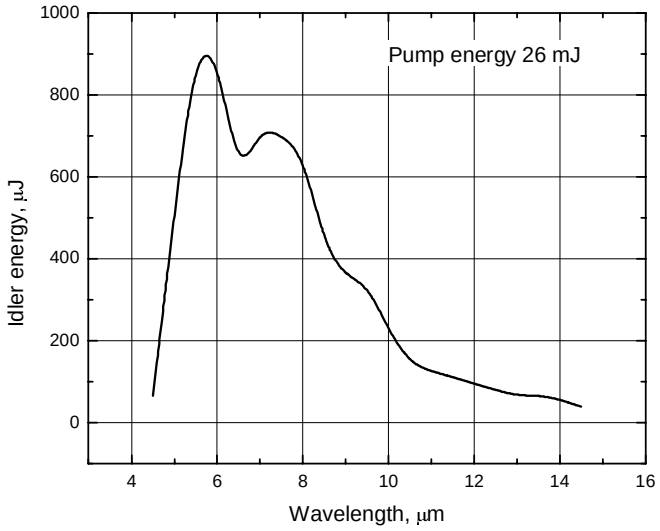

Fig.3. The tuning curve of the second stage of the tandem OPO.

The tuning curve of the second stage at 26 mJ pump energy is presented in Fig. 3. As a result, there was no crystal damage during long term measurement period in this setup, while pump intensities were as high as 20 MW/cm^2.
A low damage threshold was the one of the main reasons for limited use of $AgGaSe_2$ crystal in mid-IR OPO and lidar systems. For reliable operation of the whole spectroscopic system, some balance between performance of the OPO and damage risk must be found. Because higher idler energies can be achieved by other choices of cavity and beam parameters [10], this configuration of second stage OPO was chosen to minimize the risk of damage.
Spectral bandwidth of the mid-IR radiation was less than 10 cm^{-1} in wavelength tuning range, with typical values of 7-8 cm^{-1}. Luckily, as it is mentioned in [11], a numerous complex molecules in the atmosphere have bandwidths larger than 15 cm^{-1}. So, moderate bandwidth of the source effectively integrates background clutter rising from fine structure of atmospheric absorption found in atmospheric windows [11]. So this type of OPO could be regarded as a cost-effective source for spectroscopy of complex molecules of chemical agents.

2.2. Photoacoustic (PA) spectrometer.
For excitation of photoacoustic spectra we used the nanosecond mid-IR OPO described in previous section. More often in PA devices are used sinusoidaly modulated radiation and a resonant cells. In the pulsed photoacoustics, the system is illuminated with a laser pulse rather than with periodic modulation. Unlike non-resonant and resonant detection, which are performed in the frequency domain with periodic modulation and lock-in detection, pulsed photoacoustic detection is performed in the time domain. A pulsed cell usually possesses a single, high-Q resonant peak, so the acoustic signal is a decaying sine wave. Despite losing lock-in signal registration, the pulsed excitation possesses other advantages. Namely, the first advantage is that this technique is insensitive to the shifts in the resonant frequency, caused by volatile conditions during measurement time (gas pressure, concentration, temperature, etc.). The sensitivity lost by the removal of lock-in detection in this case can be partially compensated by usage of an extremely high Q resonator. Another advantage of pulsed PA experiments is high-energies of Q-switched lasers compared to electromechanically modulated kHz sources (PA signal is proportional to pulse energy).
In our experiments we used the photoacoustic non-resonant cell made of a massive aluminum body.

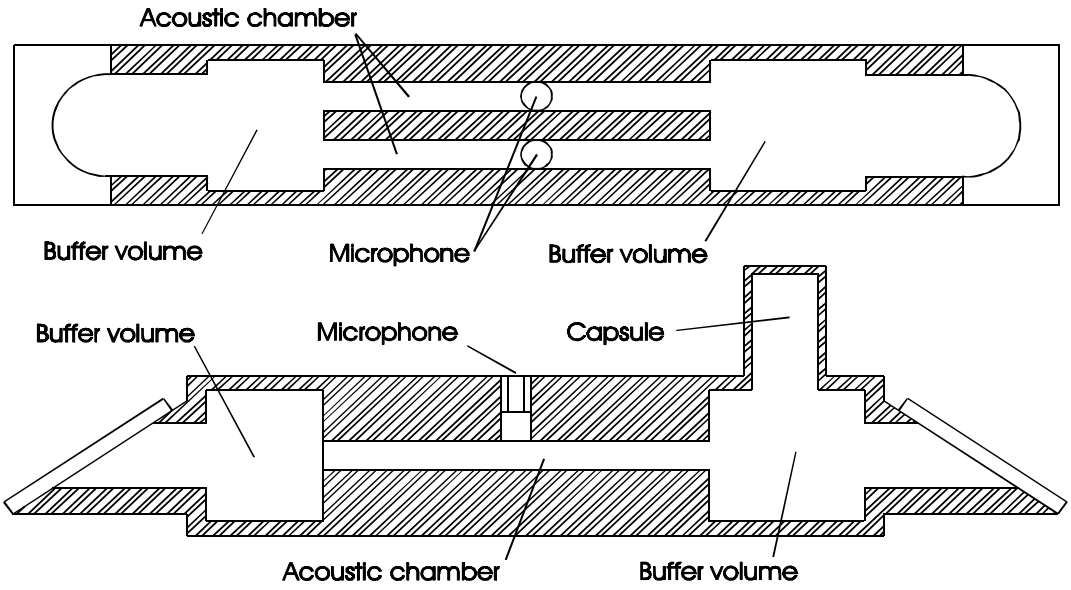

Fig. 4. Construction of the photoacoustic cell.

As one can see from Fig.4 the PA cell consists of two acoustic chambers separated by a wall. The length of the chamber is 100 mm and the diameter 7.8mm. These chambers are identical and one is used for measurement, the other one is for the reference signal. Cylindrically shaped acoustic chambers were accompanied by the buffer volumes arranged at the cell ends, approximately 30 cm^3 each. The cell has gas inlets on the side-walls of the buffer volume at each end of the cell. This allows arranging a flow-through system. The detailed explanation of PA cell construction was presented earlier [12].Each chamber has an opening in its wall for a microphone. The sensitivity of these electret microphones is 12 mV/Pa.
The laser beam enters and leaves the cells through theKRS6 windows mounted at the Brewster angle to avoid additional shot noise, energy loss and back-reflections into the cell. The laser beam was focused into the PA cell by using FL=15 ZnSe lens.

As the laser pulse passes through only one of the two acoustic chambers, a photoacoustic signal is recorded only in one of the microphones, whereas another is used for the reference signal. Both signals were filtered by the second order 40dB band-pass Butterworth filter. The center frequency of the filter was selected to be 1630 Hz. This frequency corresponds to the first resonant frequency of the PA cell. The frequency is determined by applying Fourier transform to the experimentally obtained acoustic signal. It can also be calculated as follows [13]:

$$f_n = \frac{nc}{2(l + \Delta l)}, \quad n = 1,2,3...$$

where l is the length of the chamber and c the speed of sound, Δl is the end correction factor. Small discrepancies between measured and calculated frequencies could be attributed to this factor.

After amplification both signals were supplied to the input of the differential amplifier and to the ADC200/100 converter (PicoTechnologies). Later this digitized signal was processed by PC.

2.3. Open path lidar system

Basic optical setup of the lidar is presented in Fig. 5 and Fig. 6. Opto-mechanical setup is based on the coaxial transmitter-receiver system consisting of several mirrors and lenses. The choice of these elements strongly influences main technical characteristics of the lidar: sensitivity and detection range. Some of the main advantages of this kind of coaxial transmitter - receiver system are: a simplified design, compactness, ease of adjustment, decreased cost due to the use of single mirror and large magnification of the transmitter telescope resulting in small outgoing beam divergences.
The main mirror of Newtonian telescope is a 250 mm diameter gold-coated parabolic mirror (f = 1250 mm, surface

quality – λ/8 at visible wavelengths). In addition, f = 70mm ZnSe lens and two gold mirrors are used for transmitting outgoing radiation. Incoming radiation is focused by the main mirror to the detector. One quarter of the main mirror area is used for transmitting outgoing radiation and other 3/4 for receiving incoming radiation. For sharp focusing of backward radiation into the small area detector we use additional short focal length ZnSe lens. The additional prism can be introduced into the infrared beam path. Together with an objective it serves as a viewfinder showing exactly the view formed by the main mirror. In general, all elements in this setup are specially chosen according to the properties of the laser radiation of our source and specifications of the detector.

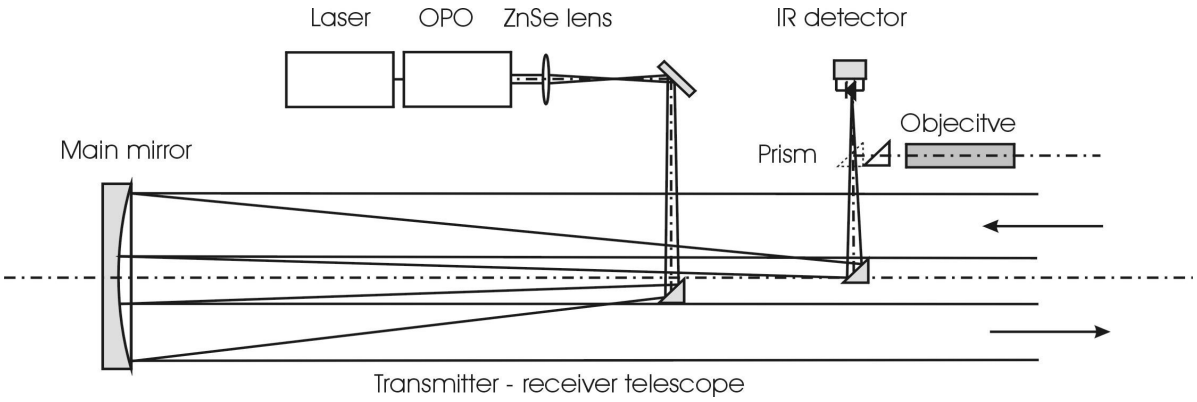

Fig.5. Basic optical setup of the lidar

Two types of detectors are used in our experiments: pyroelectric and MCT. For long - path measurements we obtained thermoelectrically cooled MCT detectors ($D^*=10^{10}$cm $Hz^{1/2}/W$, $\Delta\nu$=200 MHz) with high sensitivity and low NEP. For lidar test measurements even pyroelectric detectors ensured sufficient signal/noise ratio.
However, sensitivity of both detector types was insufficient to detect radiation scattered from aerosols. Retroreflectors are usually employed in such circumstances. We manufactured a large aperture retroreflector, maintained on a stable tripod. This retroreflector consists of three perpendicularly oriented 150mm gold mirrors with protective coatings. Our primary experiments showed that the usage of the retroreflector enables significant extension of the detection range.
The aiming mechanism and mechanical adjustable mounts for optics of the lidar system are mounted on a mobile steel table. The aiming mechanism can be scanned over 360 deg in azimuth, + 90 deg in a positive elevation. The construction of the table is chosen to be as stable as possible but it should allow easy adjustment of the lidar. This was achieved with the help of adjustment system employing two conical bearings and helical adjusters.

III. EXPERIMENTAL RESULTS

Both the PA and lidar signals, wavelength of OPO, spectra recording were processed by PC using LabVIEW (National Instruments) based software.
First, the OPO source was used for photoacoustic measurements. The beam was directed into the upper acoustic chamber. To test the functioning of the whole system we recorded PA spectrum of not-calibrated concentration of methane. Resulting photoacoustic spectra are in good agreement with that from HITRAN data and are presented in Fig.6. Estimated concentration of methane was several thousands ppmv. As the final goal of our project is detection of atmospheric pollutants and other hazardous materials, the next step was registering spectra of various nitro compounds. As an example, a spectra of 6600ppmv concentration 2-Nitropropane are presented in Fig. 7. We estimated that sensitivities of several ppm and less could be reached with this PA spectrometer.
The PA spectra were also used for testing the calibration of the OPO wavelength. As it is pointed out in [14], sometimes discrepancies between generated and those calculated with published Sellmeier coefficients may appear. So we used PA spectra of six nitro compounds (Nitromethane, Nitroethane, 1-nitropropane, 2-nitropropane, Nitrobenzene, 4-nitrotoluene) and their reference spectra [15] to test the wavelength of the OPO. To resolve the peaks the spectral derivation of both measured and reference spectra to the second derivative was used [16]. Spectra derivation is advantageous for several reasons. Enhanced resolution is achieved to allow the peak separation. And, contrary to the

first derivatives, the second derivatives do not change peak structure of spectra. After derivation, the peak of the primary spectrum is converted to the peak of derivated spectrum, although with the opposite sign.

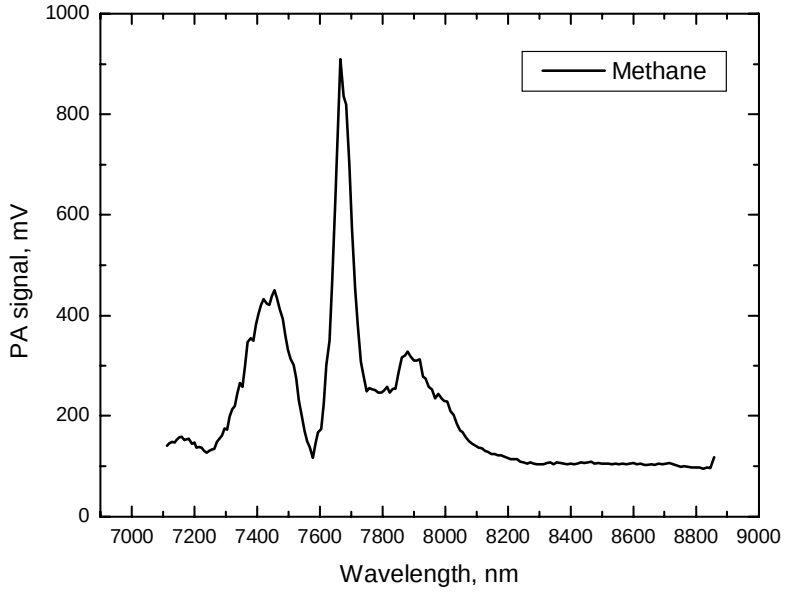

Fig.6 PA spectrum of methane.

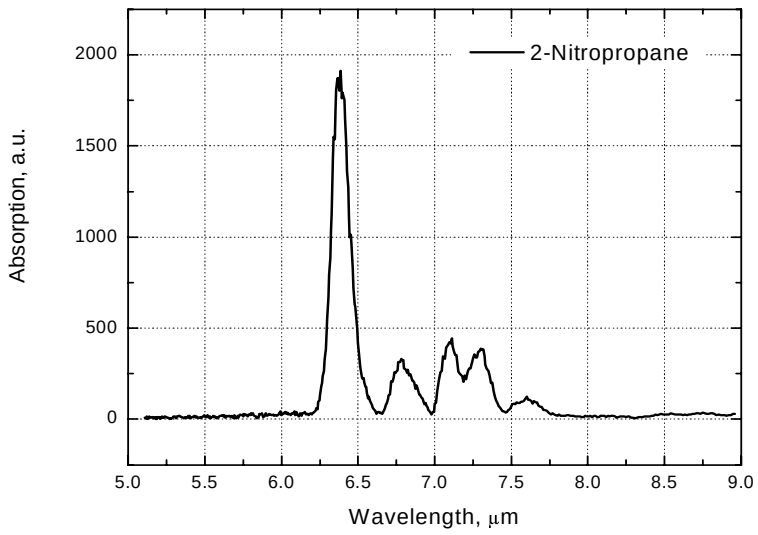

Fig.7. PA spectrum of 2-Nitropropane.

Results of peak detection are shown in Figure 8. 22 peaks in the 6000 – 8500 nm range were resolved both from measured and from reference spectra sheets. Linear approximation by the least square method was applied to these points. This line is in good agreement with the $AgGaSe_2$ OPO phase-matching curve calculated with Sellmeier coefficients [17]. Difference between the linear approximation of position of peaks, experimental points and phase-matching curve is comparable with OPO radiation spectral bandwidth, i.e. less than 10 cm^{-1}. This difference increases from the -8.8 cm^{-1} at 6.15 μm to the 8.8 cm^{-1} at 7.27 μm. Experimental points are distributed randomly around linear fit with standard deviation 4.45 cm^{-1}, that is twice smaller than the OPO radiation spectral bandwidth. This approach could also be used during the lidar operation to check wavelength calibration.

When the OPO was integrated into the lidar, the first stand-off measurements using lidar were performed. The beam path of 50 – 250 m was used for initial experiments. At first, we recorded absorption spectra of ammonia. The reflection from gold mirror (30x20 mm) was used for returning radiation making the total beam path 50 m. 5 cm^3 of ammonia (10%) water solution were inserted into a cylindrical cell (diameter 320 mm, length 500 mm) with thin polyethylene film windows. The surface area of the solution was made as large as possible so ammonia could evaporate. The resulting vapor spectrum in the 8.0 – 13μm region was recorded. It is presented in Fig 9. The PA spectrum of the ammonia is presented above. There is a good agreement between the spectra and though the lidar spectrum is much nosier, still it is good enough to tell if ammonia was present in the beam path. We estimated that the use of retroreflector and MCT detectors could produce similar results with ranges up to several kilometers.
This setup does not allow using benefits of differential absorption, but it uses all wide tuning range of the OPO source. This could be useful when identification of multiple gases is desirable instead of just one as in differential absorption.

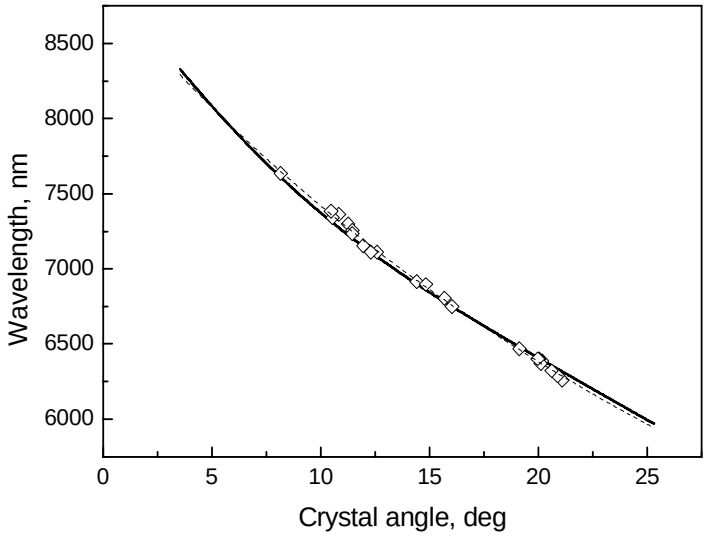

Fig. 8. Test of calibration of OPO wavelength. Diamonds are experimental points for peak positions of nitrogen compounds. Dashed line is a linear approximation of these points. Solid curve is AgGaSe2 OPO phase-matching curve. Crystal angle is given relative its cut angle.

IV. SUMMARY

Generation of continuous tunable mid-IR radiation using the two stage tandem OPO was demonstrated. Tuning of wavelength in 6 – 12 μm region was performed with pulse energies in the 0.3-1 mJ range. The designed all solid state DIAL system for mid-infrared spectral region was preliminary tested in field measurements.
Using this mid-IR OPO a trace gas detection system consisting of the photoacoustic spectrometer and the open path absorption lidar was developed and tested. PA spectra of different species were recorded. 22 peaks in the 6000 – 8500 nm range were resolved both from measured and from reference spectra sheets. They were used for lidar wavelength

calibration. Basic operation of mid-IR lidar also was demonstrated. Further improvement of the detection range as well as mounting the lidar in the truck is expected in 2006.

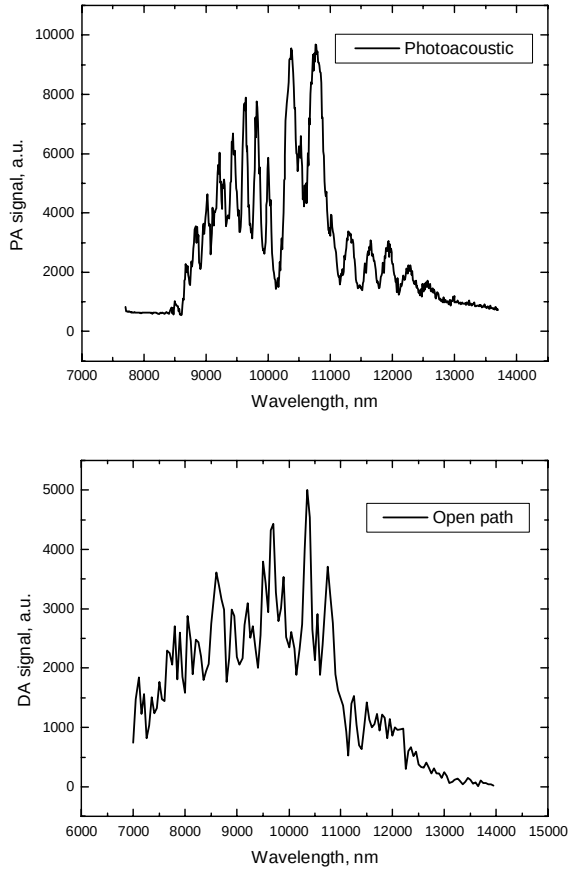

Fig.9. PA and open path spectra of ammonia

ACKNOWLEDGEMENTS

The outlined experiment is a part of program "Infrared laser based spectrometric systems for remote sensing of atmospheric pollution" (LISATNAS), supported by Lithuanian State Science and Studies foundation, Contract No B-12/2003. We also acknowledge engineer R. Skipitis for useful technical support in construction of lidar and photoacoustic spectrometer.

REFERENCES

1. D.F. Flanigan, "A short history of remote sensing of chemical agents", SPIE, Vol 2763, 2-17 (1996).
2. U. Panne, "Laser remote sensing", In: Trends in analytical chemistry. 17, 491-500 (1998).
3. E. Zanzottera, "Differential absorption lidar techniques in the determination of trace pollutants and physical parameters of the atmosphere", Crit. Rev. Anal. Chem. 21, 279-319 (1990).

4. A. Ben-David, S.L. Emery, S.W. Gotoff, and F.M. D'Amico, "High pulse repetition frequency, multiple wavelengths, pulsed CO2 lidar system for atmospheric transmission and target reflectance measurements", Appl. Opt. 31, 4224-4231 (1992).
5. C.B. Carliste, J.E. van der Laan, L.W. Carr, P. Adam, and J-p. Chiaroni. "CO2 laser-based differential absorption lidar system for range-resolved and long-range detection of chemical vapor plumes", Appl. Opt. 24, 6187-6200 (1995).
6. D.B. Cohn, W.S. Griffin, L.F. Klaras, E.J. Griffin, H.C. Marciniak, J.A. Fox, C.R. Swim, "WILDCAT sensor", SPIE, Vol 4036, 210-218 (2000).
7. F.Capasso, A.Tredicucci, C.Gmachl, D.L.Sivco, A.L.Hutchinson, A.Y.Cho, G.Scarmacio. IEEE J.Sel. Top. Quantum Electron. 5, 792 (1999).
8. M.Beck, D.Hofstetter, T.Aellen, J.Faist, U.Oesterle, M.Ilegems, E.Gini, H.Melchior. Science 295, 301 (2002).
9. P. Weibring, H. Edner, and S. Svanberg, "Versatile Mobile Lidar System for Environmental Monitoring", Appl. Opt. 42 (18), 3583-3594 (2003).
10. M. Kaučikas, Z. Kuprionis, V. Vaičikauskas. Tunnable middle IR optical parametric oscillator for spectroscopic applications. Lithuanian Journal of Physics, 45(2), 109-113 (2005).
11. Toomas H. Allik, Suresh Chandra, Wayne W. Hovis, Christopher G. Simi, James A. Hutchinson. Advances in optical parametric oscillators with application to remote chemical sensing. SPIE, Vol.3383, p. 58-64 (1998).
12. M. Kaucikas, Z. Kuprionis, V. Svedas and V. Vaicikauskas. Infrared photoacoustic gas spectroscopy employing pulsed optical parametric oscillator. SPIE Proceedings Vol.5953 275-282 (2005).
13. A.Miklos, P.Hess, Z. Bozoki. Application of acoustic resonators in photoacoustic trace gas analysis and metrology. Rev.Sci.Instr. 72(4) 1937 (2001).
14. Toomas H. Allik, Suresh Chandra, Wayne W. Hovis, Christopher G. Simi, James A. Hutchinson. Advances in optical parametric oscillators with application to remote chemical sensing. SPIE, Vol. 3383, 58-64 (1998).
15. "NIST Standard Reference Database Number 69, June 2005 Release," in *NIST Chemistry WebBook*. http://webbook.nist.gov/chemistry/.
16. P. Stchur, D. Cleveland, J. Zhou and R. G. Micheli. "A review of recent applications of near infrared spectroscopy, and of the characteristics of a novel PbS CCD array-based near-infrared spectrometer," *Appl. Spectrosc. Reviews* 37, 383–428 (2002).
17. D.A. Roberts, "Dispersion equations for nonlinear optical crystals: KDP, AgGaSe2 and $AgGaS_2$", Appl. Opt. 35 (24), p.4677-4688 (1996).